Continental Shelf Research 29 (2009) 1873–1886

Contents lists available at ScienceDirect

Continental Shelf Research

journal homepage: www.elsevier.com/locate/csr

Sub-inertial characteristics of the surface flow field over the shelf of the central Mid-Atlantic Bight

Brian Dzwonkowski [a,*], Josh T. Kohut [b], Xiao-Hai Yan [a,c]

[a] College of Marine and Earth Studies, University of Delaware, Newark, DE, USA
[b] Institute of Marine and Coastal Sciences, Rutgers State University of New Jersey, New Brunswick, NJ, USA
[c] State Key Lab of Marine Environment, Xiamen University, Xiamen, China

ARTICLE INFO

Article history:
Received 14 October 2008
Received in revised form
23 March 2009
Accepted 7 July 2009
Available online 15 July 2009

Keywords:
Surface currents
Correlation scales
HF radar
Mid-Atlantic Bight
Surface velocity

ABSTRACT

Observations of surface velocity data from August 2002 to February 2004 were collected by a series of four long-range high-frequency (HF) radars along the coast of New Jersey. The shelf observations of the central Mid-Atlantic Bight (MAB) were compared to historical observations of surface flow characteristics in the area. The time-averaged spatial mean velocity of 4 cm/s in the down-shelf along-shelf direction and 3 cm/s in the offshore across-shelf direction compared very well to historical surface measurements in the study region. However, as the spatial resolution of the data set revealed, this simple measure masked significant spatial variations in the overall and seasonal mean flow structures. Three regions – the south bank of the Hudson Shelf Valley, the southern New Jersey inner shelf (LEO-15) region, and the region offshore of the Delaware Bay mouth (southwest corner) – had mean flows that favor offshore transport of surface water. In terms of temporal variability, maps of the principle axes showed that the across-shelf (minor) axis contribution was not insignificant in the surface layer ranging from 0.3 to 0.9 of along-shelf (major) axis and that there were seasonal differences in orientation and ellipticity. Analysis of the spatial changes in the temporal and spatial correlation scales over the shelf showed that shelf position, in addition to site separation, contributed to the differences in these properties. Furthermore, observations over the Hudson Shelf Valley region suggested that this was a region of transition in which the orientation of along- and across-shelf components begin to change.

1. Introduction

While there have been many studies on the hydrography of Mid-Atlantic Bight (MAB) dating back to at least the 1930s (Bigelow, 1933; Bigelow and Sears, 1935), the work over the last 30–40 years has lead to a well accepted general circulation pattern. This circulation is well summarized in a recent paper by Lentz (2008) which re-examines past observations and presents a modified theoretical model. The MAB region is dominated by a mean depth-averaged flow in the southwestward direction (down-shelf) of 5–10 cm/s with the mean vertical structure peaking at or near the surface and deceasing with depth (Bumpus, 1973; Beardsley et al., 1976; Shearman and Lentz, 2003; Rasmussen et al., 2005; Flagg et al., 2006; Lentz, 2008; among others). The observations of the across-shelf circulation are described using a layered structure, in which the surface boundary layer flows offshore and a divergence zone in the bottom boundary layer near the mid to outer shelf separates onshore flow shoreward of the divergence from offshore flow seaward of the divergence (Csanady, 1976; Lentz, 2008). Time-averaged depth-dependent profiles of many previous long-term studies shown by Lentz (2008) indicates mean across-shelf flow is weaker than along-shelf flow, with the across-shelf magnitudes ranging from 1.5 to 4 cm/s depending of the location in the water column. Peak offshore flow occurs in the surface layer, while peak onshore flow occurs in the geostrophic layer and decreases near the bottom. More specifically in the central MAB, measurements indicate along (across)-shelf flow in the *surface* layer of the mid-shelf, between 25 and 60 m isobaths, to be 4 (1.6) cm/s in the down-shelf (offshore) direction. While this general circulation pattern does explain the overarching characteristics in the MAB, the large extent of the area inevitably leads to a synoptic under sampling with numerous experiments having been conducted in limited regions and for limited durations.

In recent years, high-frequency (HF) radar along sections of the MAB coast provides an opportunity to examine smaller-scale surface flow characteristics and variability over intra-annual to inter-annual time scales. The purpose of this study is to examine

* Corresponding author.
E-mail address: briandz@udel.edu (B. Dzwonkowski).

0278-4343/$ - see front matter © 2009 Elsevier Ltd. All rights reserved.
doi:10.1016/j.csr.2009.07.005

the surface flow structure over the shelf of the central MAB at a spatial level unresolved with traditional ship-based cruises or moorings. The study focuses on an 18 month HF radar dataset, examining spatial flow structure across the MAB in the context of historical ship and mooring studies. This new dataset affords us the opportunity to examine surface current variability not previously examined in the MAB. The high resolution HF radar dataset includes time periods of high and low stratification and regions of distinct topographic features. Section 2 describes the study area and the data used. The reader is referred to Dzwonkowski et al. (2009); and Kohut et al. 2006; for additional background information on the HF radar data. Section 3 presents analysis of the structure and variability of the overall and seasonal mean fields, while Section 4 describes along- and across-shelf variability using the velocity time series and the spatial and temporal correlation scales of the surface flow for individual grid points in several key regions of the shelf. A discussion of the results in light of previous studies as well as this study's conclusions are presented in Sections 5 and 6.

2. Site and data

2.1. Study region

While the focus of this study is the central MAB off the coast of New Jersey, a broader view of the surrounding region reveals several notable features that complicate the flow structure. Two major geographic/bathymetric features of the region are the Hudson shelf valley/Hudson Canyon and the change in coastline orientation at Long Island (Fig. 1). The Hudson shelf valley/Hudson Canyon extends across the entire shelf dramatically warping the bathymetric contours as the mouth of the Hudson River is approached. This coincides with a shift in coastline orientation from approximately 54° (counter clockwise from east) along the New Jersey coast to approximately 10° along the Long Island coast. This change in orientation impacts the flow and presents difficulties in determining along- and across-shelf coordinates over the northern section of the study area. In addition to these geographic and bathymetric features, the effects of buoyancy discharge from the Hudson River estuary have been shown to be unusually extensive throughout the study region (Yankowsky and Garvine, 1998; Tilburg and Garvine, 2003; Chant et al., 2008a, b; Castelao et al. 2008).

Over the years, there have been a number of experiments conducted in this region with many of the historic works summarized by Beardsley and Boicourt (1981) and Lentz (2008). In addition, there have been several recent programs that are relevant to this study. The majority of recent work has focused on the inner shelf starting with the NJUP experiment in the summer of 1996 and several other studies centered on the Long-term Ecosystem Observatory at 15 m (LEO-15). In late 2003, a Rutgers University autonomous underwater vehicle project began collecting temperature, salinity, and optical data along a regular transect known as the Endurance Line (Fig. 1, blue dashed line) which starts in the inner shelf and extents to the shelf break. Furthermore, the Langrangian Transport and Transformation Experiment (LaTTE), a multiple year project from 2004–2006, examined physical, chemical, and biological dynamics of the Hudson River outflow. This work complements these previous studies by providing surface current information further offshore with long-term coverage not previous available.

2.2. HF radar surface currents

This study used 4.55 MHz long-range, HF radar data from a region of the central MAB off the coast of New Jersey (Fig. 2). The

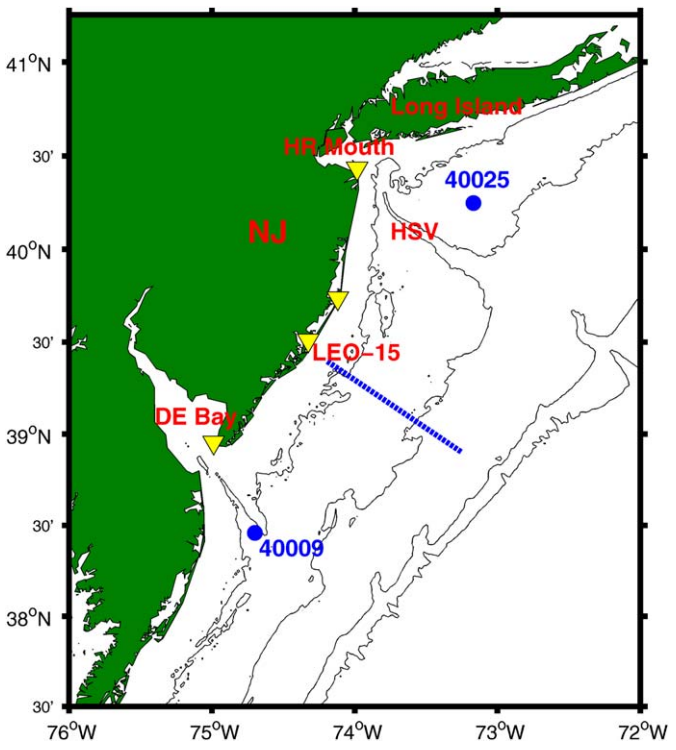

Fig. 1. Map of the central MAB showing bathymetry (black lines), HF radar sites (yellow triangles), NOAA buoys (blue circles) and the Endurance line (blue dotted line). In addition, several regions of reference are labeled, where HR Mouth is the Hudson River Mouth, HSV is the Hudson Shelf Valley, LEO-15 is the Long-term Ecosystem Observatory at 15 m, NJ is New Jersey, and DE Bay is the Delaware Bay

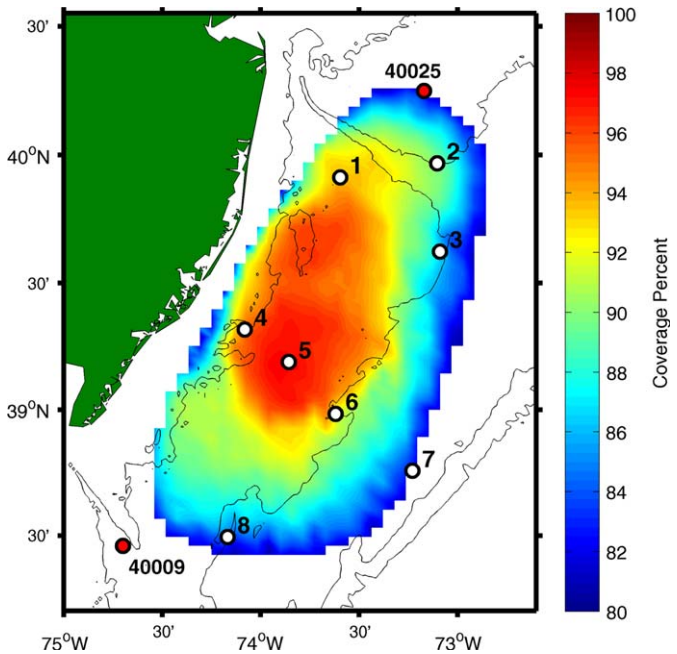

Fig. 2. The percent coverage of the HF radar network and the locations of 8 individual study sites. The percent coverage (coloration plot) is percent of valid velocity data contained in the 18 month long time series at each grid point in the coverage areas of 80% or greater. The eight study sites are individual HF radar grid points indicated by the white circles with the black outlines labeled one through eight. Wind data from NOAA environment buoys are shown as red circles with black outlines and labeled in black.

radial vectors collected by the HF radar array were averaged and geometrically combined onto a grid of UV component velocity vectors produced every 3 h following Kohut et al. (2006) and Gong et al. (2009). With an operating frequency of 4.55 MHz, the effective depth of the surface velocity measurement is approximately 2.4 m (Stewart and Joy, 1974) and the distance between grid points was in the order of 6 km. The surface current data was processed and operated in accordance with community recommendations. In particular, any data with geometric dilution of precision (GDOP) values greater than 1.5 were removed. Based on comparisons between radial current vectors from the HF radar and in situ ADCP and drifters (Kohut et al., 2006; O'donnell et al., 2005; Ullman et al., 2006), these data have an expected uncertainty on the order of 5–10 cm/s.

2.3. Surface winds

Wind data from a number of regional sources were collected over the same time period as the current data. The primary wind data used in this study were collected from NOAA buoy #44025 (Long Island (LI) wind) and NOAA buoy #44009 (Delaware Bay (DB) wind), at the northern and southern regions of the HF radar data (http://www.ndbc.noaa.gov/) (Fig. 2). In general, the hourly data were continuous over the 18 month period; however the LI wind had a considerable gap during May/June of 2003. This gap was filled using data from NOAA buoy #44017 (Montauk Point) with an appropriate transfer coefficient and lag applied to each component. In addition, the wind data was subsampled to match the 3 h HF radar data after the low-pass filtering discussed in the next section. As the NOAA buoys border the study region, a mean wind velocity time series for the study was created by vector averaging the LI and DE buoy wind data. Only minor deviations from the original two time series were present (low-frequency vector correlation between buoy sites: $r = 0.88$, $\theta = 5^\circ$, transfer coefficient $= 0.84$, and lag $= 0$ h). From this mean wind vector, surface wind stress was estimated following Large and Pond (1981).

2.4. Data analysis

As this study focuses on the mean flow patterns and low-frequency characteristics of the surface layer currents, the mean and standard deviation (std.) are calculated only when the time series have 80% data coverage. Fig. 2 shows the 80% coverage area of the HF radar network for the 18 month time period of this study (August 15 2002–February 5 2004). The study uses several mean calculations with the time-averaged mean being the mean over the stated period at each HF radar grid point, the spatial mean being the mean over the HF radar footprint, and the time-averaged spatial mean being the time average of the spatial means. The means were computed as vector averages (mean of each component then combined), and the complex std. is computed as $\sigma = \sqrt{\sigma_u^2 + \sigma_v^2}$where σ is the std. of each component.

To isolate the low-frequency signal in the HF radar data, a 40 h low pass Lanzcos filter was used to remove tidal and near-inertial signals. Prior to filtering, any gaps in the data were filled using temporal-linear interpolation. This scheme is adequate since the study was concerned with the low-frequency characteristics; and on average only 6% the temporal gaps in the time series were longer than 12 h. This is similar in concept to a study of low-frequency coastal processes by Dever et al. (2006), which interpolated through gaps in ADCP data of 19 h or less.

Using the filtered data, several characteristics of the low-frequency flow were examined. Principle axes were calculated at each HF radar grid point to determine the primary direction and orientation that maximized the temporal variability at each grid point. Following Chant et al. (2004), the current vectors were rotated 54° counterclockwise from east so that along- and across-shelf components can be analyzed separately. In addition, time series from several individual grid points, discussed below, were used to determine temporal scales, velocity component correlations, and spatial scales. The decorrelation time scale was defined to be the time that the correlation function takes to drop below $1/e$ (e-folding time scale) with the correlation function being the time lagged autocorrelation of the time series. Thus, the correlation function is simply the correlation coefficient plotted as a function of time, where time reflects the lag in autocorrelation calculation. Spatial correlations were determined using set points and calculating the correlation coefficient with the other HF radar grid points resulting in distributions of r-values over the HF radar footprint.

The specified grid points examined in this study were selected so that along- and across-shelf variability of key regions of the shelf could be investigated. The sites are shown in Fig. 2 with Sites 1–3 lying in the direct vicinity of the Hudson Shelf Valley, Site 4–7 lying along the 'Endurance line' (a region of uniformly orientated isobath that Rutgers University regularly runs AUV's along), and Site 8, which is at the base at the southern edge of the HF radar footprint. It should be noted that Sites 2, 3, 6, and 8 approximately follow the 50 m isobath, forming an along-shelf transect and that the Endurance line sites form an across-shelf transect. These stations will be referred to throughout the following sections as they were used to look at some of the spatial and temporal variability in more detail.

In addition to the total 18 month data set (August 15 2002–February 5 2004), two seasonal periods were examined. The results of previous studies in and near this region (Lentz, 2001; Kohut et al., 2004; Rasmussen et al., 2005; Castelao et al., 2008), and AUV measured across-shelf sections of temperature and salinity (October 2003–October 2004) showed that the water is typically strongly stratified during the summer months (June, July, August, September) and relatively well mixed during the winter months (December, January, February, March). Thus, the data were divided into a stratified (June 2003–September 2003) and mixed period (December 2002–March 2003) reflecting these observations. These temporal divisions affect the degrees-of-freedom (DOF) used in determining the significance of the correlation coefficient. A decorrelation time scale of two days was used to determine the DOF for each period. This is an overly conservative value as most of the time series in the HF radar grid have decorrelation time scales of 1–1.25 days as discussed below. Consequently, the DOF for each time period are 265 for the total, 61 for the stratified period, and 60 for the mixed period. The correlations reported in the following were significant at the 95% confidence level unless stated otherwise.

It should be pointed out that analyzing a data set of this size has a several caveats. First, there is some difficulties in establishing the 'along' and 'across' orientation of the surface vectors. Given the complex bathymetry, sharp changes in coastline orientation, and seasonal variability in the principle axes in the northern portion of the HF radar footprint (shown below), there are potential arguments against any of the typical means of objectively selecting the 'along' and 'across' shelf directions. Thus, an orientation as determined by Chant et al. (2004) (54° counterclockwise from east) that is reasonable for the bulk of the HF radar footprint was used from which changes observed in the assumed orientations are noted and discussed.

In an attempt to avoid 'along' and 'across' shelf terminology, both the temporal and spatial complex correlations were examined. However, when compared to the component

correlations, the complex correlations were typically dominated by the 'along-shelf' component in nearly all cases. The complex correlation generally appeared to be a slight modulation of the 'along-shelf' correlation which largely masked the variability seen in the 'across-shelf' component, even at the sites around the Hudson Shelf Valley. The dominance of the along-shelf component in a coastal region is not unexpected as several studies (Pettigrew, 1981; Dever, 1997; Dever et al. (2006), etc.) have commented the along-shelf component can overwhelm the relatively weaker across-shelf component when analyzed in vector form. However, it is somewhat surprising that in the orientationally ambiguous northern region, the 'along-shelf' component still largely dominates the complex spatial correlation. That being said, the rotational component provided by vector analysis was well captured by the rotation observed in the principle component analysis (discussed below). Consequently, the component analyses combined with the principal axis analysis provided the necessary information in the most succinct manor.

In addition, since the HF radar data is a geometric combination of radial component vectors from 4 sites along the coast (red triangles; Fig. 1), the resolution of the radial currents vary from the inner shelf to the outer shelf. When these radials are combined to totals, the grid points further offshore are based on fewer vectors with lower spatial resolution than the higher resolution radials near-shore. Across the grid the resolution of a given vector is therefore at least the scale of the diameter of the search radius in the combination step (20 km in our case) with the potential for slightly larger scales near the offshore edges of the coverage. Consequently, the spatial correlation maps resulting from this study should be viewed in this context from which descriptive differences can be attributed to separation distance and/or position differences. That being said, this study focuses on changes in regions of high correlation, arbitrarily chosen as r-values greater than 0.75. This was done because the spatial scales defined by the $1/e$ cutoff are larger than the study region in several cases, particularly in the along-shelf direction. Furthermore, the spatial averaging involved in the processing of the HF radar data has potential for smearing smaller-scale velocity shears, a feature observed in previous studies in the Hudson Shelf Valley (Harris et al., 2003).

3. General and seasonal surface patterns

To establish a general sense of the overall flow structure in the study area a few basic statistics were examined. Table 1 shows the time-averaged spatial mean of the current and time-averaged wind for the total time period and the mixed and stratified periods. During the total and mixed1 periods, the wind was from the northwest and strong (>0.03 Pa), while the surface current tended to be southward, with the mixed period being more south–southeastward. The stratified period had weak south winds, but southward current similar to the mixed period despite the change in wind conditions. While these results were not surprising, the HF radar data allows for a much more detailed view of the mean and variability of the surface currents.

Table 1
Magnitude and direction of the wind stress and the time averaged spatial mean over the HF radar grid during the total (August 15 2002–February 5 2004), mixed (December 02–March 03) and stratified (June 03–September 03) periods.

Total	Magnitude	Direction (deg.)
Current (cm/s)	5	179
Wind stress (Pa)	0.03	131
Mixed		
Current (cm/s)	5	168
Wind stress (Pa)	0.05	132
Stratified		
Current (cm/s)	3	175
Wind stress (Pa)	0.01	340

The direction is in compass degrees with the along-shelf axis being 36°/216° and the offshore direction being −126°.

The spatial variability in the time-averaged mean flow structure is shown in Fig. 3 with the time-averaged mean of each grid point (Fig. 3a) and their complex std. (Fig. 3b). The mean velocity plot shows that the flow structure had regions of south/southwest flow between 4–7 cm/s, largely in the southern region of the HF radar footprint beyond the 25 m isobath. However, the flow structure was not always parallel with local isobaths as there was a slight offshore veering of the vectors. Furthermore, there was a north to south trend of gradually increasing velocity in the flow field with mean velocity values of 2–3 cm/s in the north and 5–7 cm/s in the south. More importantly, the spatial resolution of the observations revealed several distinct flow structures, one just south of Hudson Shelf Valley, previously identified by a Rutgers University (RU) team (Chant et al., 2008a, b; Castelao et al., 2008) and another at the southern edge of the study region. In addition, the outer edges of the Long-term Ecosystem Observatory at 15 m (LEO-15) study area (39° 25′N, 74° 15′W) appeared to have a significant across-shelf component in the time-averaged mean velocity. While the plot for the time-averaged mean velocity provided a general picture of the surface flow, the std. illustrates that most of the surface current energy is in the variability about that mean. In Fig. 3b, the std. was three to four times the magnitude of the mean velocity and generally increased with distance offshore. The northeast region of the HF radar footprint had the lowest std. values and again, similar to the mean plot, there was a general increase in the std. in the southward direction. However, this increase in value was not as smooth as in the mean plot.

3.1. Mixed response

The time-averaged mean flow structure for the mixed period is in Fig. 4a. The mixed period time-averaged mean structure looked very similar to the total time-averaged mean structure with the velocity magnitudes being somewhat stronger than the total period and the vectors in the southern region tending to veer more offshore. Hence, the general flow direction was more southward, rather than the south–southwestward of the total period.

As more information about flow variance can be obtained from the principle axes, the temporal variability at each grid point was summarized in this way for the two seasonal periods (Fig. 4). During the mixed period (Fig. 5a), the major axes had magnitudes of around 10–16 cm/s and were generally stronger than the minor axes ($\cong 6$ cm/s), which gave the flow variance a relatively rectilinear appearance. The major axes were orientated in the along-shelf direction with most axis orientations lying between 40° and 60° (along-shelf angle 54°). Thus, while the time-averaged mean of the grid point was not along isobaths, the variability (principle axes) was largely oriented along the isobaths. Only in the northwest corner (between the 25 and 50 m isobaths) of the study region were the major and minor axes nearly equal. In addition, the effects of the corner geometry of the study area were seen in the region north of the Hudson Shelf Valley where the axis orientation rotated around by 30–50°. This is more in line with the east–west coast of Long Island.

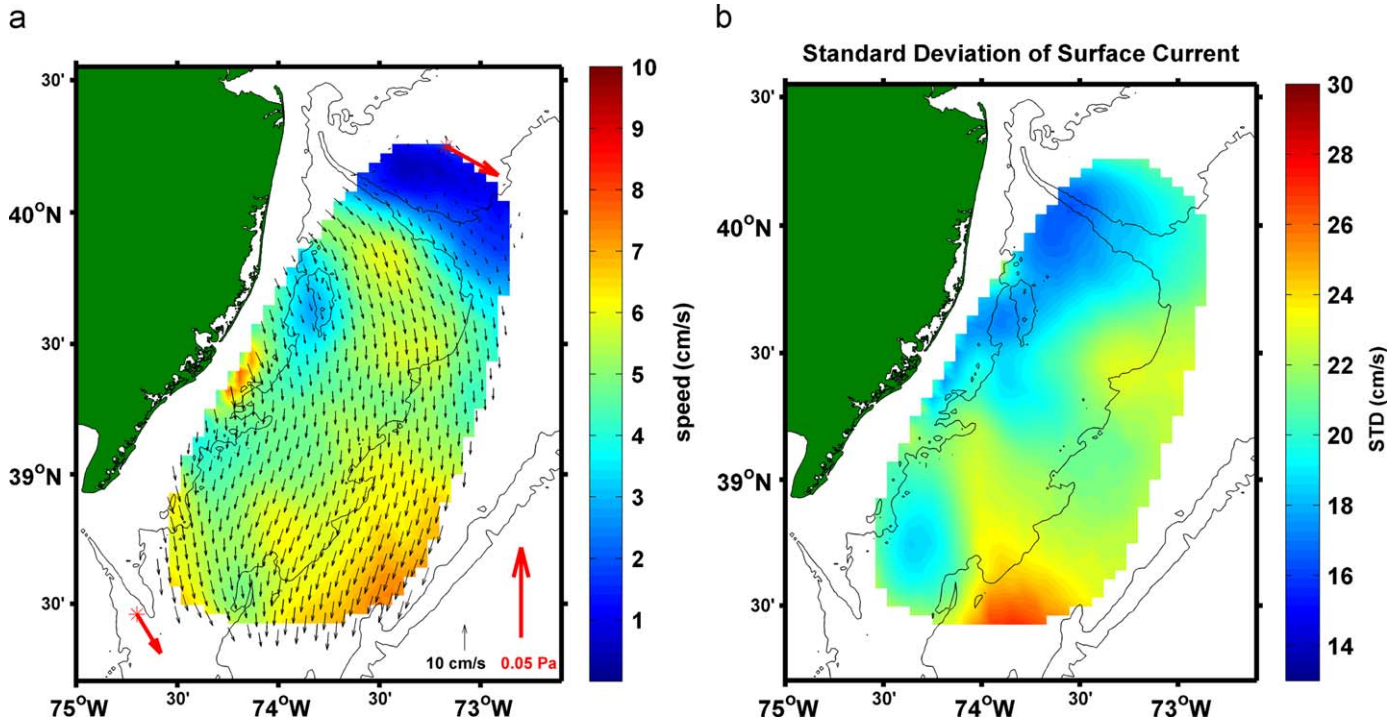

Fig. 3. (a) and (b) The time-averaged mean of each grid point (a) and their stand deviation (std.) (b) over the total period in the study area. In the mean plot, the black arrows are current velocities and the coloration is current magnitude (cm/s). The coloration in the right plot is the complex std. in cm/s. The red arrows are the mean wind stress at the NOAA environment buoys used in the study region.

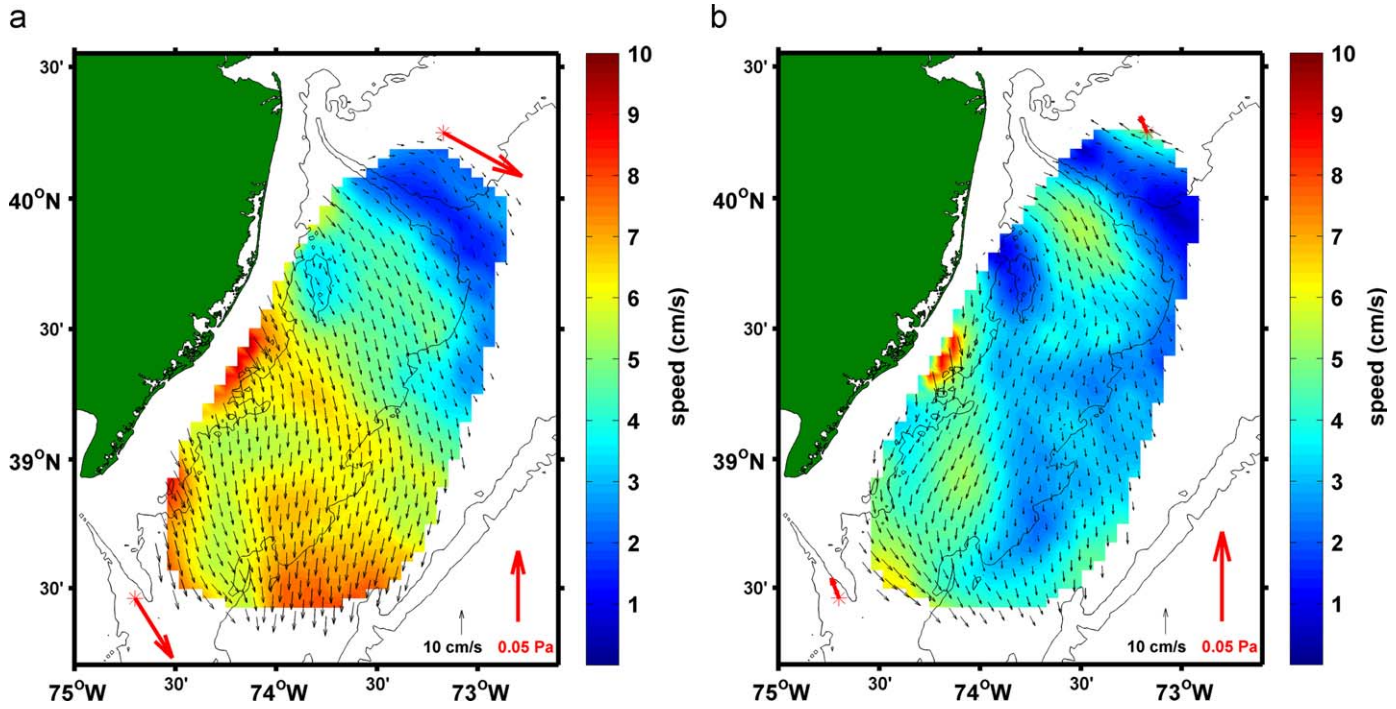

Fig. 4. (a) and (b) The time-averaged mean during the mixed and stratified periods temporal (a) and (b), respectively. The black arrows are current velocities and the coloration is current magnitude (cm/s). The red arrows are the mean wind stress during the respective time period at the NOAA environment buoys used in the study region.

3.2. *Stratified response*

The time-averaged mean flow structure for the stratified period is in Fig. 4b. The flow magnitudes tended to be between 1–5 cm/s. Again, there were three regions of distinct flow similar to those of the total period description mentioned above. However, the velocity differences between these regions and the surrounding grid points were larger, making these features more

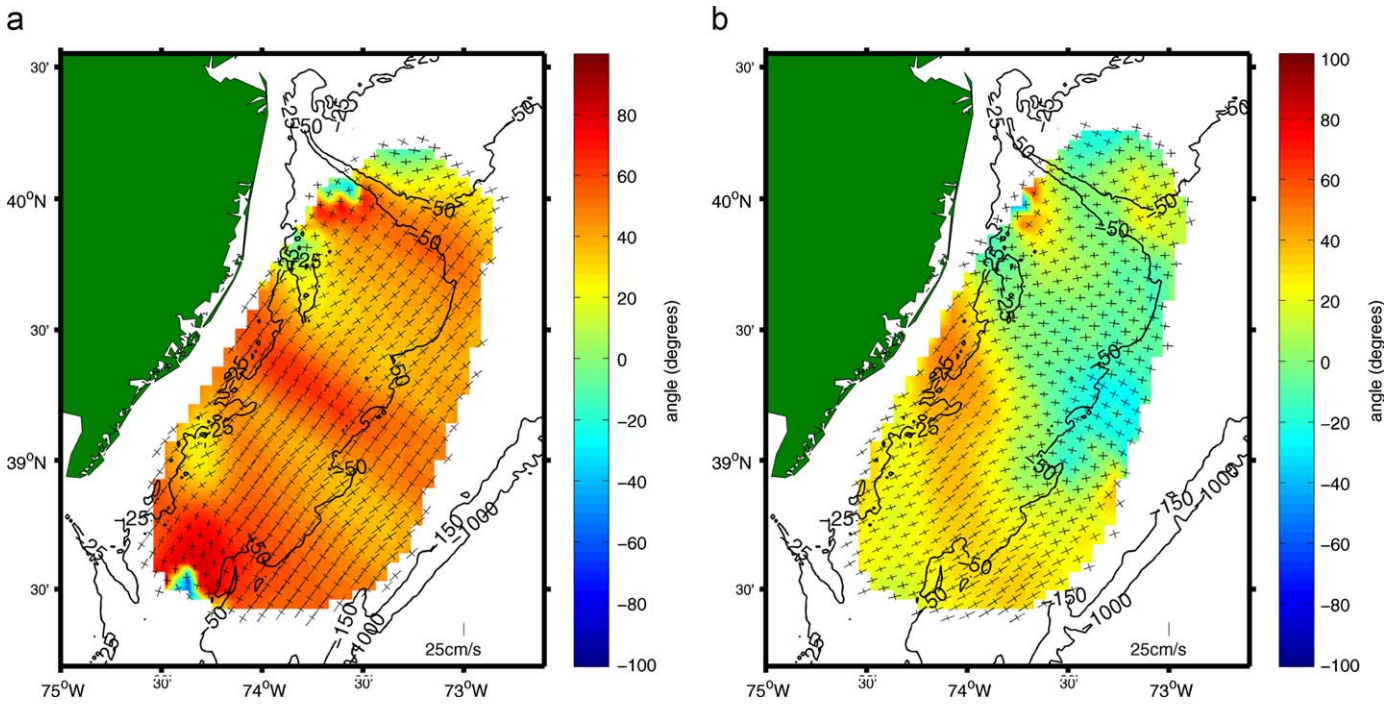

Fig. 5. (a) and (b) The principle axis at each grid point for the mixed and stratified seasonal periods (a and b, respectively). The principle axes of the low-frequency velocity of the HF radar data (after temporal linear interpolation) are shown with the black crosses being the major and minor axis and the coloration representing the angle orientation of the major axis counterclockwise from east.

notable. In addition, outside of this LEO-15 and southwestern flow regions, the mean current direction tended to be parallel to local isobaths.

The principle axes during the stratified period are shown in Fig. 5b. The major (minor) axes magnitudes were approximately 8–12 cm/s (4–7 cm/s), with the southwest half of the study region favoring the major axis and the northeast half of the study region having a much more circular structure. In addition, the principle axes experienced a gradual rotation with the southwest region having an orientation of 25–45° and the northeast region being 10° to −15°.

4. Along- and across-shelf variability

The spatial differences over the HF radar footprint were further compared using the eight site locations mentioned above to determine the temporal scales, velocity fluctuations, and spatial scales of along- and across-shelf velocity components. While the design of the site locations allowed for observations of specific areas of interest, such as the Hudson Shelf Valley, it was also useful in observing the changes of these properties in along- and across-shelf directions.

4.1. Temporal correlation scales

Before the individual velocity time series were examined, the temporal decorrelation scales were determined as these were important for obtaining the degrees-of-freedom in the scalar correlations mentioned above. Fig. 6 shows the temporal correlation functions of along- and across-shelf components of the current at the eight site locations and the corresponding wind stress (Figs. 6a and b, respectively). The temporal correlation functions showed some expected patterns for along- and across-shelf components of the current velocity and wind stress with the pattern generally following a cosine-shaped monotonic decline through the decorrelation level (thin horizontal black line). While the temporal correlation for the wind stress components were similar (29–30 h), along-shelf current velocity tended to have a larger decorrelation time and a larger temporal range than the across-shelf current velocity. Furthermore, the sites along the Endurance line (Sites 4–7) showed an increase in the temporal scale from 22 h near-shore to 30 h offshore. This was also seen further north relative to Sites 1 and 3. The time scales in the along-shelf direction as indicated by points along the 50 m isobath (excluding Site 8) showed consistent along-shelf current scales of 27–28 h. The temporal decorrelation scales in the across-shelf velocity component, however, were less consistent with values ranging from18 to 28 h.

A further investigation of these scales over the full grid revealed a complex and detailed picture of the surface flow characteristics over the shelf. The spatial structure for both along- and across-shelf velocity components over the entire HF radar grid are shown in Figs. 7a and b, respectively. As seen in the individual site analysis, the decorrelation scales of the along-shelf component generally increase with distance offshore over the entire grid. The inner shelf area (around the 25 m isobaths) tended to have values of 20–24 h, the mid-shelf (25–50 m) tended to have values of 24–28 h, and the middle to outer shelf (50–100 m) tended to be 28–32 h. However, there were some exceptions, particularly along the Hudson Shelf Valley, which had longer decorrelation time scales closer to shore as can be seen by the yellow/orange coloration along its path.

The apparent relationship between depth and temporal decorrelation time did not appear to hold for the across-shelf component. In Fig. 7b, in general, the across-shelf temporal decorrelation times were shorter than those seen in the along-shelf component with the longest just north of the Hudson Shelf Valley. This is likely due in part to the changing orientation of the coastline in this location, making our cross-shelf component more consistent with the along-shelf analysis further south along the New Jersey coast.

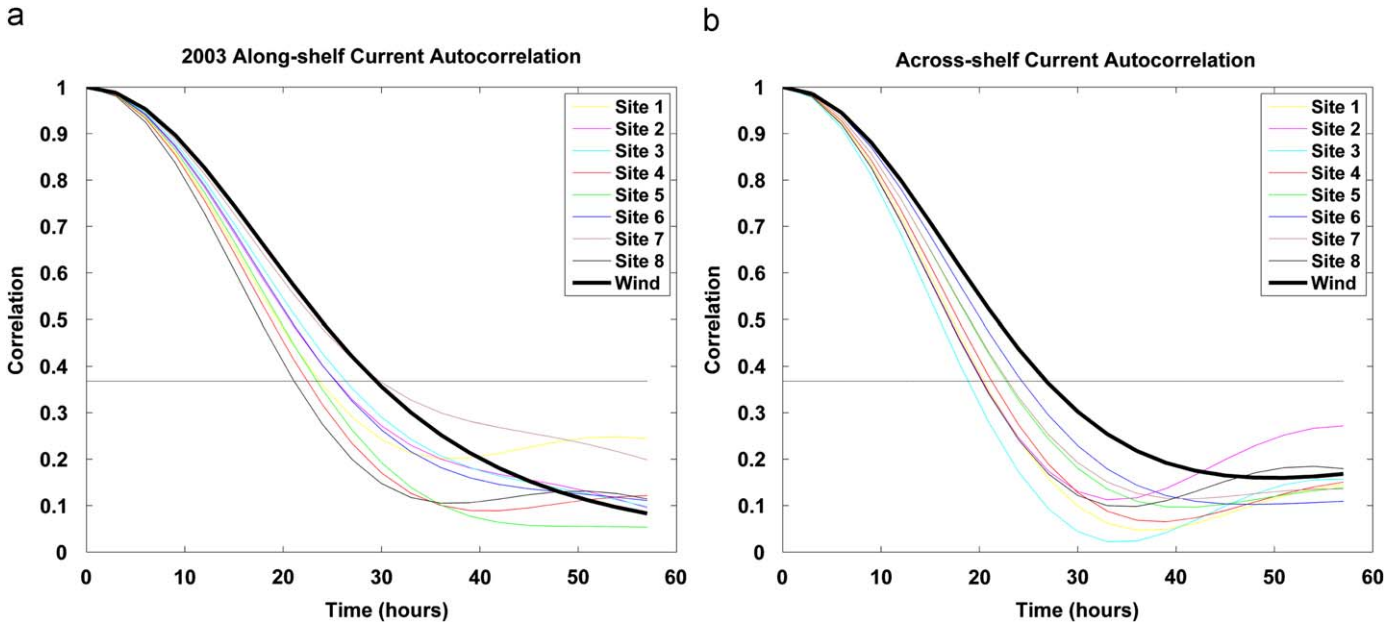

Fig. 6. (a) and (b) The temporal correlation functions from along- and across-shelf components of the current at the eight site locations and from the wind stress (a and b, respectively). The thin horizontal black line indicates the *r*-value below which the correlation is considered un-correlated. The individual sites and wind stress are showed by the various colors.

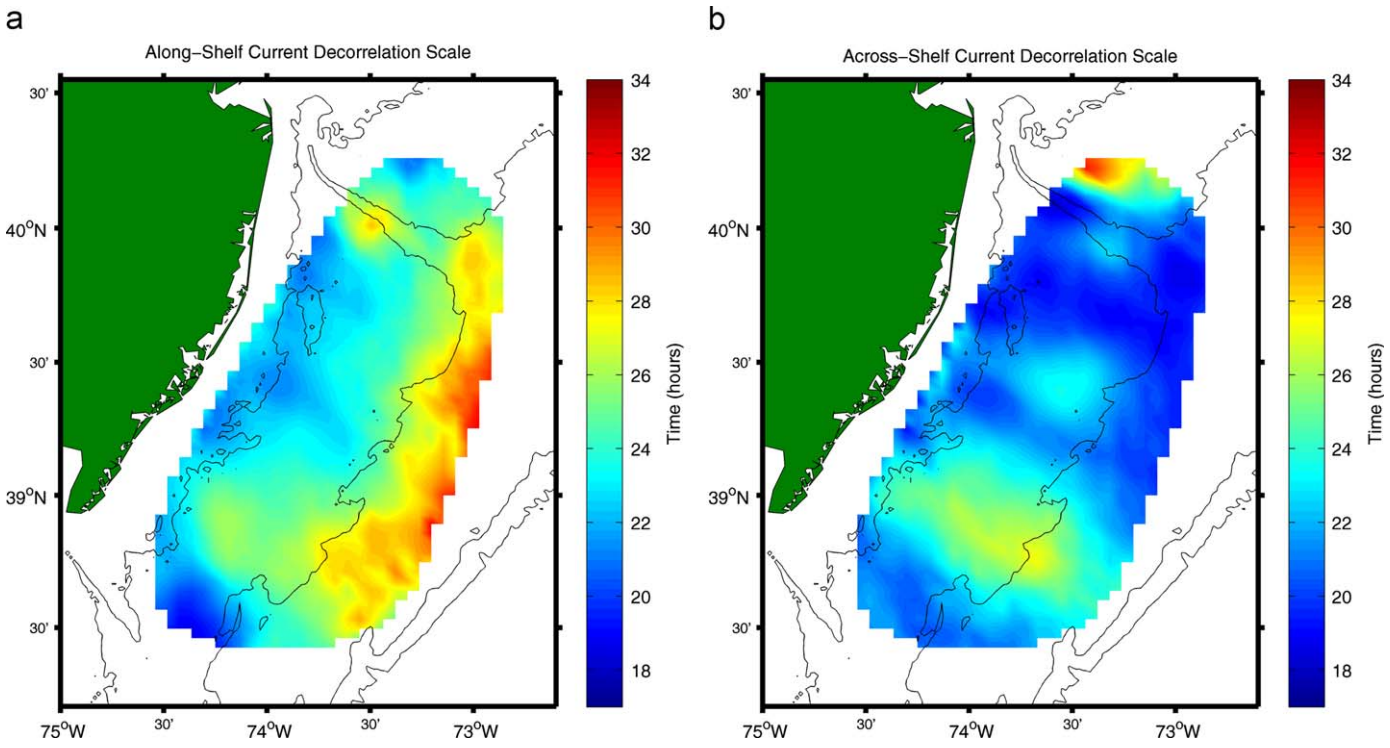

Fig. 7. (a) and (b) The decorrelation timescale over the HF radar grid for along- and across-shelf velocity (a and b, respectively). The coloration indicates the length of the decorrelation timescale.

4.2. *Velocity time series*

The time series of along- and across-shelf components over the entire study period (August 02–January 04) for Site 4 and 6 are shown in Figs. 7 and 8, respectively. The positive (negative) values in Fig. 8 correspond to up-shelf (down-shelf) flow and the onshore and offshore current in Fig. 9, respectively. In general, the along-shelf (across)-shelf components experienced fluctuations of O(40 cm/s) (O(20 cm/s)), but were well correlated at the two sites. The along (across)-shelf velocity at Sites 4 and 6 had a correlation coefficient of 0.76 (0.78) with Site 4 leading Site 6 by 3 h (0 h). There were some differences in the component magnitudes between the two sites; with Site 4 (Site 6) typically having stronger peaks in the along-shelf (across-shelf) flow. This difference was captured by their component std. While the complex sub-inertial stds. were similar, 16.7 cm/s (Site 4) and

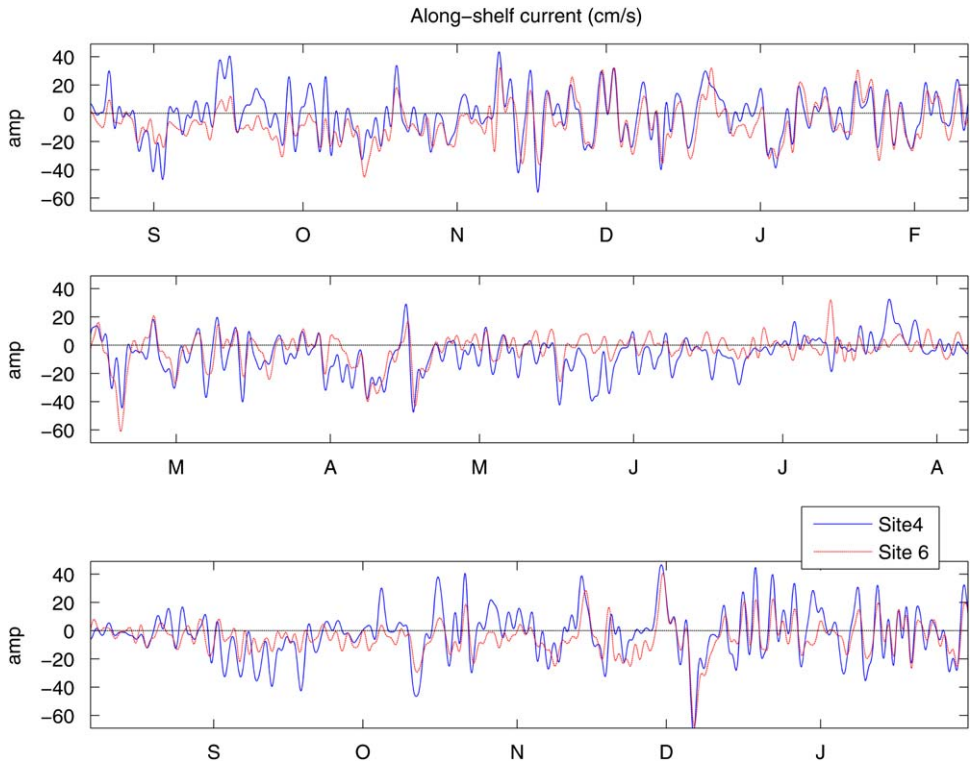

Fig. 8. Time series of the sub-inertial along-shelf component for Site 4 (blue) and 6 (red dash) over the duration of the study period (August 02–January 04). The positive (negative) values correspond to up-shelf (down-shelf) flow. The black dashed line is the zero line.

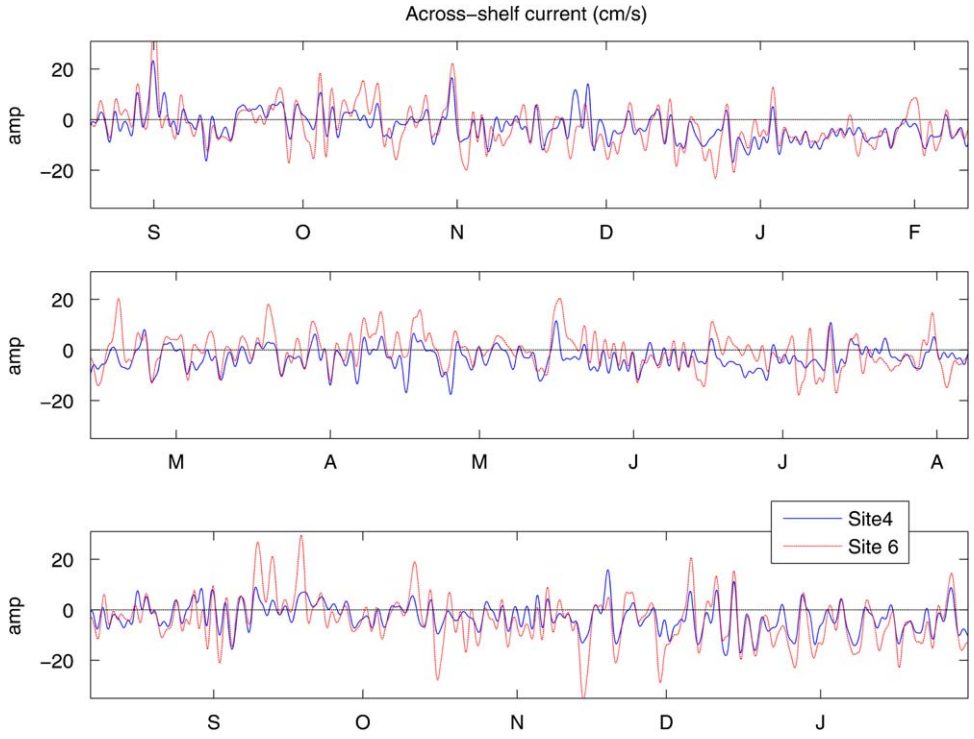

Fig. 9. Time series of the sub-inertial across-shelf component, similar to Fig. 8. The positive (negative) values correspond to onshore (offshore) current.

14.4 cm/s (Site 6), the individual components showed that the along-shelf std. is higher at Site 4 (16 cm/s compared to 12 cm/s) and the across-shelf std was higher at Site 6 (8 compared to 5 cm/s). In addition, there were periods when the across-shelf current underwent periods of consecutive offshore bursts with zero to small onshore velocities separating them (December 02, January 03, Mid-October 03–Mid-November 03, Mid-December 03–January 04).

Interestingly, there appeared to be a relationship between the across-shelf flow at Site 6 and the along-shelf flow at Site 4 (r-value $= -0.71$). A good example of this occurred in September 2003, where three large pulses of onshore flow at Site 6 were

associated with strong pulses of down-shelf flow at Site 4. During these pulses, the across-shelf flow between Site 6 and 4 was dramatically reduced, dropping from peaks of 20–30 cm/s at Site 6 to peaks of 5–8 cm/s at Site 4, suggesting strong convergence in this area, with the converging water possibly flowing south at Site 4 as opposed to subducting. As illustrated in that example, there were occurrences of very strong across-shelf currents (20–35 cm/s) which were of the order of the along-shelf currents.

Further north closer to the Hudson Shelf Valley, Sites 1 and 3 showed similar but slightly less consistent relationships in the respective along- and across-shelf comparisons (not shown). The *r*-values for the along (across)-shelf current correlation between sites was 0.69 (0.65). However, these sites did not have a high correlation between along- and across-shelf currents as seen between Sites 4 and 6.

4.3. Spatial correlation scales

Maps of spatial correlations were grouped in two ways to illustrate the differences observed throughout the HF radar footprint. Sites 4–6, along the Endurance line, is a region with relatively uniform isobaths that parallel the coast (Figs. 10 and 12). In contrast, Sites 1–3 surround the Hudson Shelf Valley, a region of more complex bathymetry (Figs. 11 and 13).

4.3.1. Along-shelf velocity correlations

In general, the spatial scales of the along-shelf velocity extend over a large portion of the HF radar footprint with the along-shelf correlation length scale being longer than the across-shelf scale. Across the endurance line (Fig. 10), there were relatively minor changes in the width, length, and magnitude of the regions of high correlations (r-value >0.75, yellow to red color), which suggest that along-shelf velocity correlations are a function of separation rather than position. However, in the area around the Hudson Shelf Valley, the structure of the spatial correlations was less uniform (Fig. 11). The spatial correlations of the seaward locations (Site 2 and 3) were similar, covering a large section of the HF footprint. The structures were less uniform and weaker in magnitude when compared to the Endurance line stations. The shoreward location (Site 1) had a much smaller region of high correlation, confined to a circular region bounded by the 25 and 50 isobath. However, it was still well correlated (0.6–0.75) over a

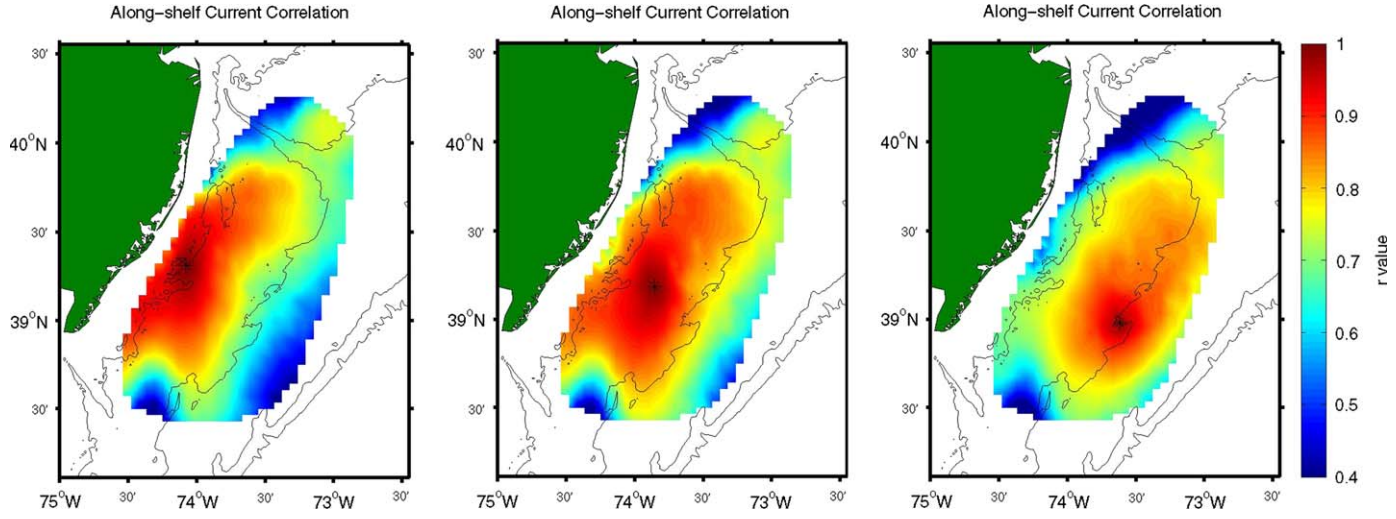

Fig. 10. The maps of the spatial correlation for the along-shelf velocities from three points (Sites 4–6) along the Endurance line with the coloration being the correlation coefficient (*r*-value) and the black star indicating the site location. The site plots are shown from the nearest to shore in the left plot (Site 4) to furthest offshore in the right plot (Site 6).

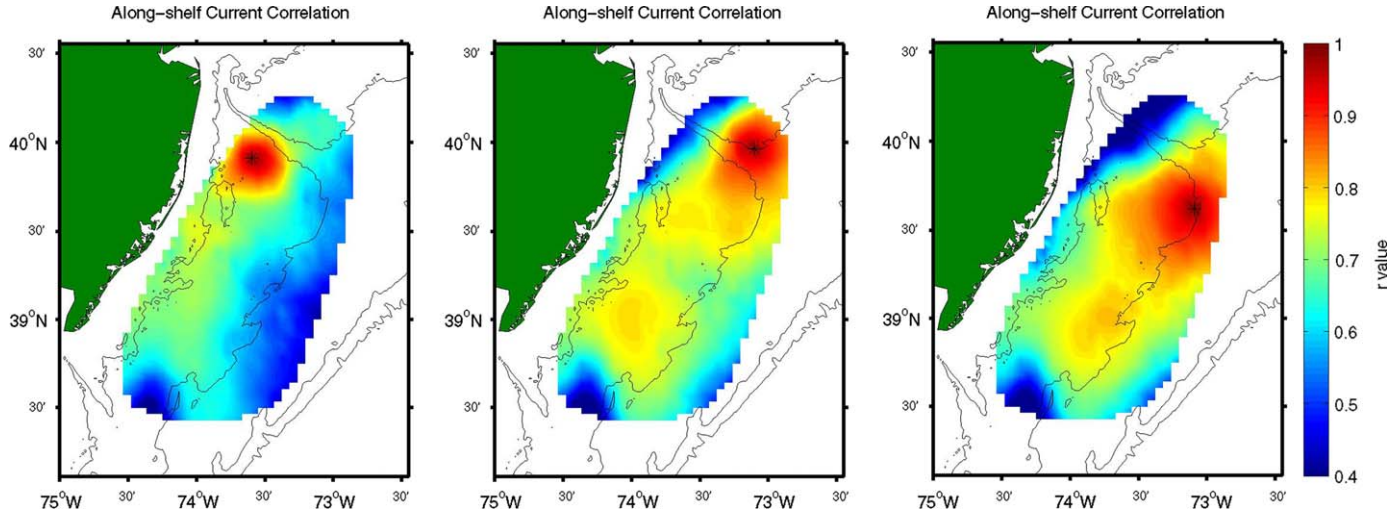

Fig. 11. Same as Fig. 10, except the along-shelf velocity correlation maps are shown for Sites 1, 3, and 2, respectively.

large portion of the shelf. These differences in structure around the Hudson Shelf Valley suggest the spatial correlation were functions of position rather separation. The points at the outer edge of the HF radar footprint (Sites 7 and 8, not shown) were somewhat more limited in there spatial scales, which could be due to their association with the study region boundary or regional processes such as the shelf break front, in the case of Site 7. This is further discussed in Section 5.

4.3.2. *Across-shelf velocity correlations*

The general patterns of the spatial correlations of the across-shelf velocity were smaller and increased with distance offshore. Fig. 12 shows the spatial correlations of the across-shelf velocity from the same sites shown in Fig. 10. At the 25 m isobath (Site 4, left most plot), the region of high correlation was centered closely around the site location with an approximate diameter of 24–30 km. While moving 24 km offshore of Site 5 the scale nearly doubled to approximately 54–60 km (78–84 km) in the along-shelf (across-shelf) direction. This scale continued to increase further offshore at Site 6 on the 50 m isobath with the along-shelf width of the high correlation region being approximately 90 km and the across-shelf width being greater than 96 km (limited by the study boundary). In addition, the spatial correlation structure at Site 7 (not shown) was very similar to Site 6 with slightly reduced along- and across-shelf widths from what can be determined given the site proximity to the edge of the HF radar footprint. It is worth noting that there was a low correlation band over the Hudson Shelf Valley region at all the sites in Fig. 12 which suggest the Hudson Shelf Valley does exert some influence over the surface flow. Further evidence of the Hudson Shelf Valley's influence appeared in two of the sites around the Hudson Shelf Valley. Both Sites 1 and 2 have a very similar spatial structure that appeared partially constrained on their north and south sides, respectively, by the southern 50 m isobath of the canyon. However, the correlation pattern around Site 3 appeared similar to Site 5, rather then Sites 2 6 (which are also on the 50 m isobath), with little apparent influenced by the Hudson Shelf Valley. Comparing Figs. 12 and 13, the shoreward sites (Sites 1 and 4) had slightly longer across-shelf correlation scales and relatively sharp boundaries. While further offshore the spatial scales increased in length, and more gradually decreased away from the site location. These differences suggests that, in addition to site separation, the shelf position also influences the spatial correlation patterns of the across-shelf velocity, even in regions of simple bathymetry such as the endurance line. This is reasonable since it would be expected that the spatial scales would change as the forcing dynamics change moving from the inner to outer shelf.

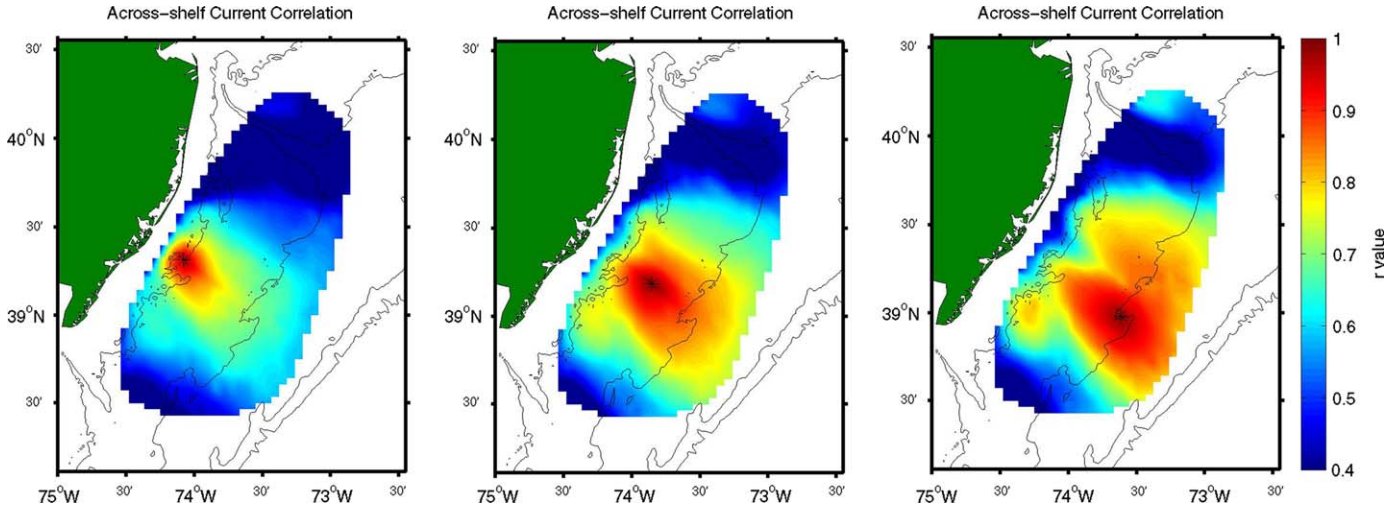

Fig. 12. Same as Fig. 10, except the across-shelf velocity correlation maps are shown.

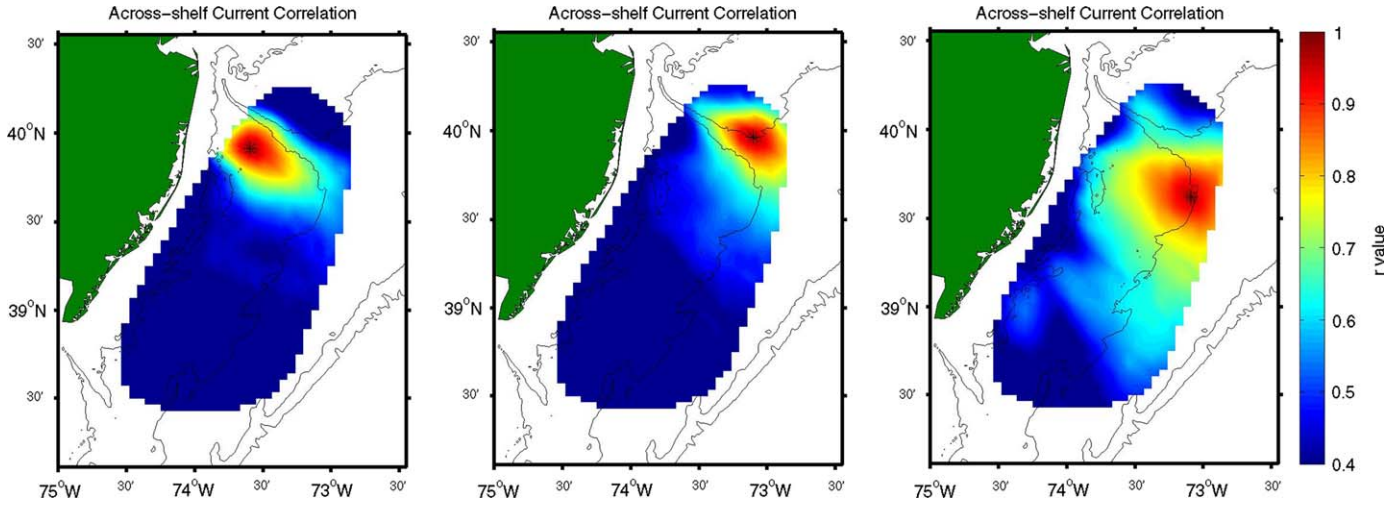

Fig. 13. Same as Fig. 11, except the across-shelf velocity correlation maps are shown.

5. Discussion

5.1. Mean and seasonal considerations

The various analyses over the HF radar footprint showed the importance of the across-shelf velocity in the surface layer. In terms of components, along- and across-shelf components of the time-averaged spatial mean are −4 and −3 cm/s, respectively, similar to long-term means previously published for the MAB (Lentz, 2008). The strong offshore component in the mean surface flow is consistent with Lentz (2008) and Csanady (1976) idealized 2-D model for mean shelf circulation. However, the spatial plot of the time-averaged velocities showed that the velocity vectors in the study region varied in magnitude and direction with the southern region of the Hudson Shelf Valley, the LEO-15 study area, and the southwest corner displaying stronger offshore flow than along-shelf flow. These features would be difficult to capture in a model that assumes along-shelf invariance. Furthermore, the std. and principle components (not shown for the total period) of the HF radar demonstrated that there were large variation around this mean flow pattern and that the across-shelf contribution was not insignificant in the surface layer. A comparison of the magnitude of the major and minor axis showed that the minor axis (across-shelf) ranged from 0.3 to 0.9 of major axis (along-shelf) depending on season and location.

Dividing the data set into mixed and stratified periods revealed notable differences. The mixed period time-averaged mean currents tended to be similar to the total period in both the magnitude and principle axes, with the vectors tending to have a stronger across-shelf component. The stratified period had weaker time-averaged mean currents, generally in the along-shelf direction with the Hudson Shelf Valley flow being more distinct. This seasonal difference in current magnitude is likely due to differences in wind stress with mean wind during the winter (0.05 Pa) significantly stronger than observed in the summer (0.01 Pa), Table 1. In addition, moving northeastward over the study area, the principle axes of the velocity grid points showed a distinct modulation, becoming less rectilinear and rotating axis orientation.

The observed variability of the principal components within and between different periods is unexpected; however, there is some limited historical evidence that agrees with the HF radar observations. Using several days to many months of surface current meter data from five mooring sites on the shelf to the south of the Hudson Shelf Valley, primarily during the fall and winter months, Mayer (1982b) observed principal component magnitudes of 13–24 cm/s (7–9 cm/s) in the major (minor) axis and variability in the orientation ranging from 32° to 51° counter clockwise from east. This is similar to the variability observed in the mixed period principal axes (Fig. 5b). These results are similar to what would be expected of depth-averaged current (i.e., along-shelf dominated with orientation following local isobaths), and Mayer (1982b) speculated that observed variability was associated with surface wind effects. Wind forcing was also seen to significantly influence the spatial flow patterns across the bight over multi-year climatologies (Gong et al., 2009).

The stratified period has more significant changes throughout the HF radar footprint. Münchow and Chant (2000) showed that surface current data during the stratified period from several moorings along the 20 m isobath in the LEO-15 study region had orientation angles of 20–30°, which agrees well with the HF radar data in that region. In addition, it is speculated that the transition of the principal axes going northward across the HF radar footprint could be related to buoyant outflow from the Hudson River as recent studies have shown the presence of its discharge over a significant portion of the shelf at times (Chant et al., 2008a, b; Castelao et al., 2008). This in conjunction with seasonal upwelling winds (Southwest winds), which Dzwonkowski et al. (2009) showed are significantly correlated to across-shelf HF radar currents and sea-level fluctuations during the stratified period ($r = 0.81$ and 0.85, respectively), could lead to the preferential change in the axis ratio (becomes more circular) and the rotation of the orientation as the across-shelf component becomes stronger relative to the along-shelf component. In addition, buoyancy outflow during the summer months may enhance stratification in the north/northwest region, which is known to play a critical role in the surface currents response to forcing mechanisms. In particular, seasonal differences in the surface current response to wind forcing on the inner shelf and shelf has been presented by Kohut et al. (2004) and Dzwonkowski et al. (2009), respectively. Several studies (Münchow and Chant, 2000; Sanders and Garvine, 2001; Garvine, 2004) in the LEO-15 region during the stratified summer season suggest/found that interior currents were in wind thermal wind balance over the shallow inner shelf (10–20 m) which suggests that stratification limits the effects of bottom friction in the water column during this time period. Along similar lines, Lentz (2001), and several others (Kirincich et al., 2005; Gutierrez et al., 2006) have stated that stratification and its relationship to eddy viscosity explain the differences observed in coastal circulation during different water column states. Thus, the observed seasonal differences in the surface current principal axes are reasonable.

Observations in the area of the Hudson Shelf Valley are particularly interesting as they add a new level of detail to the relatively complex flow region. As pointed out by Lentz (2008), there have been several previous studies examining currents in the Hudson Shelf Valley (Nelsen et al., 1978; Mayer, 1982a; Manning et al., 1994; Harris et al., 2003). However, the bulk of these studies examine bottom and/or depth-averaged currents with only very limited measurements of the surface currents. While most of these studies show mean flow (bottom and/or depth-averaged) going up-valley, the surface flow in the area around the Hudson Shelf Valley was observed to be complex, with Mayer (1982a) noting that surface velocities between two moorings, one in and the other adjacent to the Hudson Shelf Valley, could vary in direction by nearly 180° on time scales of 30 days. Since the bottom and depth-average mean current is in the up-valley direction, it should not be unexpected that there is mean surface flow down-valley in its vicinity. That being said, several recent studies (Chant et al., 2008a, b; Castelao, 2008), and several more in preparation, which have examined estuary outflow and consequently surface flow in much more detail around the mouth of the Hudson estuary and along the Hudson Shelf Valley region. These studies provide support for the strong down-valley mean flow observed on the southern edge of the Hudson Valley Shelf, which is related to buoyancy discharge.

While the total period and seasonally averaged velocities are important for understanding the general circulation, they understate the episodic nature of the surface shelf flow. This is well illustrated in the velocity plots for Sites 4 and 6. Of particular interest is the across-shelf component of Sites 4 and 6, which showed strong and frequent across-shelf flow events, O(30 cm/s). These strong, episodic across-shelf flows have the potential to transport nutrients, fresh water, and plankton significant distances offshore. Even more interesting was the increase in the along-shelf current with decreasing distance toward the coast in conjunction with a highly correlated decrease in across-shelf velocity. This relationship in the surface currents at these two sites suggest that across-shelf divergence could result in along-shelf acceleration near-shore in the area around the Endurance line. This could suggest that across-shelf convergences and

divergences in this region may not always result in conventional upwelling or downwelling.

While small scale convergences and divergences have been observed on the inner shelf of the LEO-15 region (Tilburg and Garvine, 2003; Yankovsky et al., 2000), the occurrences noted in the HF radar data appear to have a larger scale. Examining a snapshot of the low pass HF radar velocities during one of the onshore events provides additional information about the spatial extent and variability in the flow field (Fig. 14). The snapshot is preceded by a relative strong northeast wind at both NOAA National Data Buoy Center (NDBC) buoys, however the current response is quite variable with minimum (maximum) velocities in the northern (central and southern) section of the HF radar footprint and some patchiness in terms of magnitude variability. As noted in the site data, the region around the Endurance line experiences strong onshore flow in the outer region of the shelf with increasing along-shelf current closer to the coast. The region over the Hudson Shelf Valley is largely in the down-shelf direction. To the first order, the flow in the central and southern regions appears consistent with the surface Ekman response to downwelling favorable wind stress with the mid/outer shelf surface current being approximately 45° to the right of the wind. The onshore flow converges at the coast causing an amplification of the along-shelf current. The wind forced component of these flows seen over multi-year time scales is further discussed by Gong et al. (2009). In addition to the convergence observed in the individual sites, the lagged along-shelf velocity component correlations between sites revealed that the highest *r*-values occurred when the inner shelf led the outer shelf by approximately 3 h. These results agreed with previous observations that along-shelf surface current fluctuations do not vary significantly in the across-shelf direction and that shallow water responds faster to the forcing mechanisms in this region (approximately 6 h response difference) (Chuang et al., 1979; Beardsley and Haidvogel, 1981). However, the same effect was not present in the across-shelf velocity component, where lagged time series did not improve the correlations along the Endurance line.

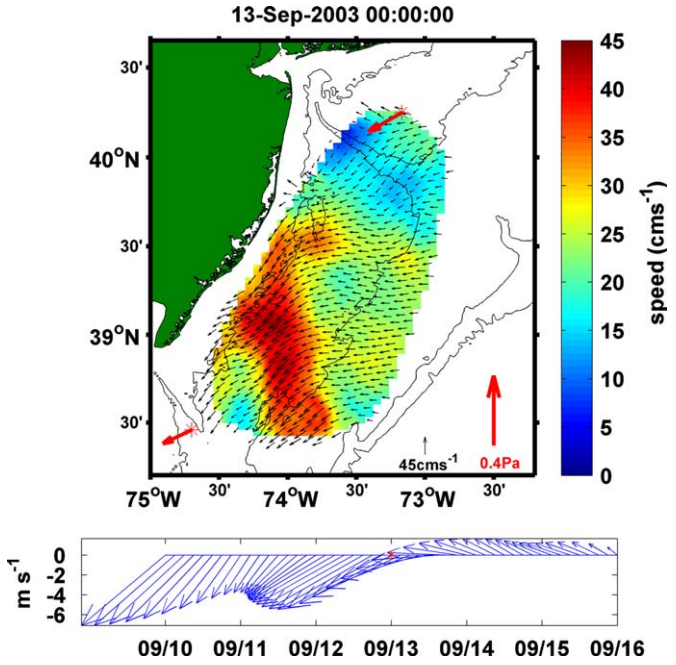

Fig. 14. Surface velocities from low-passed HF radar data for September 13 2003 00:00 UTC. Color contours of current speed (cm/s) and wind stress (red vector) are also shown. Wind vector time series for the six day interval centered on the time of the surface current map are also shown at bottom of the plot.

5.2. Characteristic of correlation scales

The temporal decorrelation scales exhibited some expected patterns over the study area. Along the Endurance line and over the shelf in general, the along-shelf decorrelation timescales increased with distance offshore, ranging from 20 to 32 h. The increased temporal decorrelation scales agreed with the notion that deep water has longer timescales. In addition, the results were similar to that of Münchow and Chant (2000) who obtained values in the surface layer of the inner shelf (20 m isobath) of the LEO-15 study area during the NJUP field experiments.

Much of the previous observational work explicitly stating the spatial scales of along- and across-shelf flow have been conducted on the west coast of the US, which has distinctly different shelf morphology than the MAB (Kundu and Allen, 1976; Winant et al., 1987; Dever 1997). As such, some differences were expected. In addition, the values used to determine spatial scales in the various studies differ to some degree, thus, the comparison between studies is qualitative. That being said, some of spatial correlations of the across-shelf currents from this study were larger then expected. Along the Endurance line and over the shelf in general, along-shelf correlation of along-shelf current were the largest, O(100 km), which is in line with theory (100–200 km; Brink et al., 1987, 1994) and observations (>60 km; Dever, 1997). There was some variability in the structure and magnitude in the Hudson Shelf Valley region as mentioned above. However, across-shelf correlation scales of the along-shelf velocity remained highly correlated for lengths of approximately 20–40 km, larger than those observed on the US west coast (10–15 km, Dever 1997). In regards to the across-shelf component, these scales showed much more site to site variability with spatial scales that were again typically larger then values on the west coast. The observed across-shelf current scales in northern California of 15–20 km (10 km) in the along-shelf (across-shelf) direction (Dever, 1997) were small compared to this studies scales of 15–50 km depending on location and when only considering the region of high correlation. Another novel observation of this study was the rapid increase in the across-shelf velocity spatial correlation over the shelf with the region of high correlation in Fig. 11 nearly tripling in width from Site 4 (25 m isobath) to Site 6 (50 m isobath).

With the exception of the along-shelf velocity along the Endurance line, the position of the various sites appeared to have a significant impact on the spatial correlations. More data is needed to link specific forcing to the detailed variability revealed in the HF radar data including, mass field measurements, high resolution sea-level and wind field data. As mentioned in Section 4.3, it was speculated that the complex bathymetry had an effect on the spatial correlations, however other processes, such as shelf break variability and buoyancy outflow, may also play a role of the positional differences in the spatial correlations. It is likely that the reduced spatial correlations at Site 7 (not shown) on the outer edge of the HF radar footprint was affected by shelf break processes. This is a plausible assumption as a recent paper by Flagg et al. (2006) showed that the along-shelf jet associated with the shelf break can impinge on the outer edges of the shelf. In fact, the reduction in correlation at the outer edges of the shelf was similarly observed off northern California, in which the reduced correlation lengths at the outmost site (130 m) compare to inner sites (60 and 90 m) were attributed to offshore mesoscale activity (Dever, 1997). In addition, the short spatial scales associated with Site 1 were possibly due to localize buoyancy outflow as this region has recently been identify as a transport pathway for the Hudson River outflow (Chant et al., 2008a, b).

Furthermore, this work suggests that the Hudson Shelf Valley represents a transition region over which the orientation of along-

and across-shelf components begin to respond to the changes in coastline orientation. The analysis of the temporal decorrelation scales showed that north of the Hudson Shelf Valley the 'across-shelf' component becomes the 'along-shelf' component as the across-shelf component has similar time scales as the along-shelf component in the southern region of the HF radar footprint. Additional evidence of this was seen in the principle axes analysis in which the orientation shifted from 40–60° to −10° to 20° and in spatial vector correlation phase plots which showed a similar rotational relationship (not shown). However, the ratio of major to minor axes in the principle components were close to one in this region indicating that a well defined along-shelf/across-shelf orientation is not present.

5.3. Forcing mechanisms

The ability of this data to determine dynamical forcing mechanisms is limited by the lack of mass field measurements and high resolution sea-level and wind field data. However, as suggested above, there are a number of likely candidate mechanisms which can be discussed. When compared to depth-averaged currents, the shallow nature of the current measurements and the spatial and temporal variability observed suggest that the measurements are sensitive to temporal and small scale spatial variability in typical forcing mechanisms. It should also be expected that these surface current measurements will be more sensitive to surface forcing such as wind stress and buoyancy discharge.

While the long-term currents are not are forced by climatological winds, the low-frequency variability in the time-averaged spatial mean of the HF radar current has been shown to be highly correlated with regional wind stress ($r = 0.65$–0.85) (Dzwonkowski et al. 2009). Furthermore, as suggested by Dever (1997), the relative large correlations in the across-shelf component suggest that the surface currents are correlated with the large-scale wind. However, in terms of smaller-scale variability, one study on the West coast of the US found that using a high resolution atmospheric model (9 km grid) revealed 10–50 km bands of strong wind stress and wind stress curl adjacent to coastal promontories, which had major impacts on the cause of offshore transport along the California coast (Pickett and Paudan, 2003). Given the relative sparse coverage of meteorological measurement stations in or around the HF radar footprint, this is an interest topic for future research that could be investigated with scatterometer data or a high resolution atmospheric model.

As stated and cited above, buoyancy forcing can also play a dynamical role over a significant portion of the shelf in this region by increasing stratification over the shelf (Castelao et al., 2008). But, it can also have significant localized impacts such as those found by Chant et al. (2008a, b) in the Hudson Shelf Valley region and by several studies in the LEO-15 region (Münchow, 1992; Yankowsky and Garvine, 1998; Tilburg and Garvine, 2003). Both of these regions have notable current patterns in the time-averaged mean figures (Figs. 3a and 4).

In addition, bathymetry also appears to contribute to localize flow variability in the flow field, with many notable studies in this region suggesting such. Song et al. (2001) showed that localize upwelling regions off the New Jersey coast could be explained using idealized bathymetry in a numerical model. Kohut et al. (2004) showed that standard range HF radar surface currents were impacted by subtle changes in bathymetry in the LEO-15 region study. In addition, several studies mentioned above indicate that the Hudson Shelf Valley also has a major impact on the shelf currents.

6. Conclusions

The overall time-averaged spatial mean is similar to previous mooring-based studies in this area, but there is significant change in the time-averaged means over the footprint of the HF radar data. In particular, there were three notable regions (the southern edge of the Hudson Shelf Valley, the LEO-15 region, and the southwest corner) that favored offshore movement of surface water, which were apparent to varying degrees in the total, mixed, and stratified periods. In addition, there were seasonal differences in the variability of the HF radar data where the principle axes rotated orientation and became more elliptical over the HF radar footprint during the stratified period. Temporal scales in the surface layer for the along (across)-shelf current ranged from 20–32 (18–28) h and appeared to be consistent with previous point measurements near the study region. The spatial scales of the along-shelf velocity were generally well correlated over the study region, consistent with studies that suggest large along-shelf spatial scales. While spatial scales of across-shelf velocity varied with location, but generally increased offshore until the outer shelf. In particular, there was a near tripling of the along-shelf width of high correlation region of across-shelf velocity moving from the 25 to 50 m isobath along the Endurance line. However, regional geography appeared to reduce the spatial correlations as seen around the Hudson Shelf Valley region, which limited the spatial scales of surface velocity. These observations, in addition to the principle component analysis suggested that the Hudson Shelf Valley region appeared to be a transition region over which the orientation of along- and across-shelf components began to respond to the changes in coastline orientation.

On the whole, three potential forcing mechanisms are speculated to be responsible for the observed small scale variability observed: buoyancy discharge; topography irregularities, both in bathymetry and in coastline orientation; and spatial wind stress variability. Adding to the challenge of dynamically analyzing high-resolution surface currents is the fact that these forcing mechanisms may not operate independently which presents the possibility of non-linear interactions. While there have been numerous studies on various continental shelves analyzing these more subtle aspects of shelf forcing, open questions remain and represent a key avenue of future research as high resolution forcing data becomes more readily available. Furthermore, these forcing mechanism are not unique to this area which suggest that the small scale features and variability observed in this region are likely common in other shelf regions.

Consequently, this study identifies significant seasonal and regional differences observed across the shelf by the time series of well resolved spatially mapped data. From the surface velocity data, several regions in the study showed characteristics consistent with the previous observations, however the level of detail provided by the HF radar data showed areas and time periods of exception. This study serves as a baseline of information for surface currents in terms of mean flow, limited seasonal variability, and temporal and spatial decorrelation scales, for which there is only limited historical data for the surface layer of this duration and spatial coverage. As such, little has been presented in terms of the spatial correlation of the across-shelf component over such an extended portion of the shelf, so the across-shelf spatial scales represent a contribution to the general oceanographic properties on continental shelves. In addition, while these spatial correlations apply to the near-surface, this work may have bearing on other levels of the water column as a study by Dever (1997) off the coast of California suggested that the correlation scales of near-surface across-shelf velocity may be applicable to interior and bottom across-shelf velocity. Finally, the regions of anomalous offshore surface flow identified in this study

have the potential of being areas of net offshore transport. These regions could play an important role in exporting material and fresh water across the continental shelf, however, as this study only had surface layer data, further investigation of these regions is needed.

Acknowledgments

This work would not have been possible without collecting, processing, and archiving the HF radar velocity maps by Coastal Ocean Observation Lab at Rutgers University, including Hugh Roarty and Scott Glenn. We also need to thank Bruce Lipphardt, Rich W. Garvine, Kuo Wong, and John T. Reager for advice and technical assistance. In addition, the two anonymous reviewers should be thanked for their valuable comments and suggestions, which have greatly improved this manuscript. This work was supported by the National Atmospheric and Oceanographic Administration through Grant #NA17EC2449 and NASA-Space Grant #NNG05GO92H.

References

Beardsley, R.C., Boicourt, W.C., Hansen, D.V., 1976. Physical oceanography of the Middle Atlantic Bight. In: Gross, M.G. (Ed.), Middle Atlantic Continental Shelf and the New York Bight. American Society of Limnology and Oceanography, Special Symposium, vol. 2. pp. 20–34.

Beardsley, R.C., Boicourt, W.C., 1981. On estuarine and continental-shelf circulation in the Middle Atlantic Bight. In: Warren, B.A., Wunsch, C. (Eds.), Evolution of Physical Oceanography, Scientific Surveys in Honor of Henry Stommel. MIT Press, pp. 198–233.

Beardsley, R.C., Haidvogel, D.B., 1981. Model studies of the wind-driven transient circulation in the Middle Atlantic Bight. Part 1: Adiabatic boundary conditions. Journal of Physical Oceanography 11, 355–375.

Bigelow, H.B., 1933. Studies of the waters on the continental shelf, Cod to Chesapeake Bay. I. the cycle of temperature. Papers on Physical Oceanography and Meteorology 2, 135.

Bigelow, H.B., Sears, M., 1935. Studies of the waters on the continental shelf, Cod to Chesapeake Bay. II. Salinity. Papers on Physical Oceanograghy and Meteorology 4, 94.

Brink, K.H., Chapman, D.C., Halliwell, G.R., 1987. A stochastic model for wind-driven currents over the continental shelf. Journal of Geophysical Research 92, 1783–1797.

Brink, K.H., LaCasce, J.J., Irish, J.D., 1994. The effect of short-scale wind variations on shelf currents. Journal of Geophysical Research 99, 3305–3314.

Bumpus, D.F., 1973. A description of the circulation on the continental shelf of the east coast of the United States. In: Warren, B.A. (Ed.), Progress in Oceanography. Pergamon Press, pp. 111–157.

Castelao, R., Glenn, S., Schofield, O., Chant, R., Wilkin, J., Kohut, J., 2008. Seasonal evolution of hydrographic fields in the Middle Atlantic Bight from glider observations. Geophysical Research Letters. doi:10.1029/2007GL032335.

Chant, R.J., Glenn, S.M., Kohut, J.T., 2004. Flow reversals during upwelling conditions on the New Jersey inner shelf. Journal of Geophysical Research 109, C12S03, doi:10.1029/2003JC001941.

Chant, R.J., Glenn, S.M., Hunter, E., Kohut, J., Chen, R.F., Houghton, R.W., Bosch, J., Schofield, O., 2008a. Bulge formation of a buoyant river outflow. Journal of Geophysical Research 113101029/2007JC004100.

Chant, R.J., Wilkin, J.J., Weifeng, Z., Choi, B., Hunter, E., Castelao, R., Glenn, S., Jurisa, J., Schofield, O., Houghton, R., Kohut, J., Frazer, T.K., Moline, M.A., 2008b. Dispersal of the Hudson River Plume on the New York Bight. Oceanography 21 (4), 149–162.

Chuang, W.-S., Wang, D.-P., Boicourt, W.C., 1979. Low-frequency current variabilities on the southern Mid-Atlantic Bight. Journal of Physical Oceanography 9, 1144–1154.

Csanady, G.T., 1976. Mean circulation in shallow seas. Journal of Geophysical Research 81, 5389–5399.

Dever, E.P., 1997. Subtidal velocity correlation scales on the northern California shelf. Journal Geophysical Research 102, 8555–8571.

Dever, E.P., Dorman, C.E., Largier, J.L., 2006. Surface boundary-layer variability off Northern California, USA, during upwelling. Deep-Sea Research 53, 2887–2905.

Dzwonkowski B., Kohut, J.T., Yan, X.H., 2009. Seasonal differences in wind-driven across-shelf forcing and response relationships in the shelf surface layer of the central Mid-Atlantic Bight. Journal of Geophysical Research, accepted.

Flagg, C.N., Dunn, M., Wang, D.P., Rossby, H.T., Benway, R.L., 2006. A study of the currents of the outer shelf and upper slope from a decade of shipboard ADCP observations in the Middle Atlantic Bight. Journal of Geophysical Research 111101029/2005JC003116.

Garvine, R.W., 2004. The vertical structure and subtidal dynamics of the inner shelf off New Jersey. Journal of Marine Research 62, 337–371.

Gong, G., Kohut, J.T., Glenn, S.M., 2009. Seasonal climatology of wind-driven circulation on the New Jersey Shelf, Journal of Geophysical Research, submitted.

Gutierrez, B.T., Voulgaris, G., Work, P.A., 2006. Cross-shore variation of wind-driven flows on the inner shelf in Long Bay, South Carolina, United States. Journal of Geophysical Research 111, C03015, doi:10.1029/2005JC003121.

Harris, C.K., Butman, B., Traykovski, P., 2003. Winter-time circulation and sediment transport in the Hudson Shelf Valley. Continental Shelf Research 23, 801–820.

Kirincich, A.R., Barth, J.A., Grantham, B.A., Menge, B.A., Lubchenco, J., 2005. Wind-driven inner-shelf circulation off central Oregon during summer. Journal of Geophysical Research 110, C10S03, doi:10.1029/2004JC002611.

Kohut, J.T., Glenn, S.M., Chant, R.J., 2004. Seasonal current variability on the New Jersey inner shelf. Journal of Geophysical Research 109, C07S07, doi:10.1029/2003JC001963.

Kohut, J.T., Roarty, H.J., Glenn, S.M., 2006. Characterizing observed environmental variability with HF doppler radar surface current mappers and acoustic doppler current profilers: environmental variability in the Coastal Ocean. IEEE Journal of Oceanic Engineering 31 (4), 876–884.

Kundu, P.K., Allen, J.S., 1976. Some three-dimensional characteristics of low-frequency current fluctuations near the Oregon coast. Journal of Physical Oceanography 6, 181–199.

Large, W.G., Pond, S., 1981. Open ocean momentum flux measurements in moderate to strong winds. Journal of Physical Oceanography 11, 324–336.

Lentz, S.J., 2001. The influence of stratification on the wind-driven cross-shelf circulation over the North Carolina shelf. Journal of Physical Oceanography 31, 2749–2760.

Lentz, S.J., 2008. Observations and a mode l of the mean circulation over the Middle Atlantic Bight Continental Shelf. Journal of Physical Oceanography 38101175/2007JPO3768.1.

Manning, J.P., Oey, L.Y., Packer, D., Vitaliano, J., Finneran, T.W., You, K.W., Fromm, S., 1994. Observations of bottom currents and estimates of resuspended sediment transport at the New York 12-mile dumpsit. Journal of Geophysical Research 99, 10221–10239.

Mayer, D.A., 1982a. Circulation in the Hudson Shelf Valley: MESA physical oceanographic studies in New York Bight, 1. Journal of Geophysical Research 87, 9563–9578.

Mayer, D.A., 1982b. The structure of circulation: MESA physical oceanographic studies in New York Bight, 2. Journal of Geophysical Research 87, 9579–9588.

Münchow, A., 1992. The formation of a buoyancy driven coastal current. Ph.D dissertation, University of Delaware, Newark, DE, 205.

Münchow, A., Chant, R.J., 2000. Kinematics of inner shelf motions during the summer stratified season off New Jersey. Journal of Physical Oceanography 30, 247–268.

Nelsen, T.A., Gadd, P.E., Clarke, T.L., 1978. Wind-induced current flow in the upper Hudson Shelf Valley. Journal of Geophysical Research 83, 6073–6081.

O'Donnell, J., Ullman, D., Spaulding, M., Howlett, E., Fake, T., Hall, P., Isaji, T., Edwards, C., Anderson, E., McClay, T., Kohut, J., Allen, A., Lester, S., Turner, C., Lewandowski, M., 2005. Intergration of Coastal Ocean Dynamics Application Radar (CODAR) and Short-Term Predictive System (STPS) Surface Currents into the Search and Rescue Optimal Planning System (SAROPS), CG-D-01-2006.

Pettigrew, N.R., 1981. The dynamics and kinematics of the coastal boundary layer off Long Island, Ph.D Thesis, Massachusetts Institute of Technology/Woods Hole Oceanographic Institute, Woods Hole, MA.

Pickett, M.H., Paduan, J.D., 2003. Ekman transport and pumping in the California current base on the US Navy's high-resolution atmospheric model (COAMPS). Journal of Geophysical Research 108 (C10), 3327, doi:10.1029/2003JC0019092.

Rasmussen, L.L., Gawarkiewicz, G., Owens, W.B., Lozier, M.S., 2005. Slope water, Gulf Stream, and seasonal influences on the southern Mid-Atlantic Bight circulation during the fall-winter transition. Journal of Geophysical Research 110101029/2004JC002311.

Sanders, T.M., Garvine, R.W., 2001. Fresh water delivery to the continental shelf and subsequent mixing: an observational study. Journal of Geophysical Research 106 (C11), 27087–27102.

Shearman, R.K., Lentz, S.J., 2003. Dynamics of mean and subtidal flow on the New England shelf. Journal of Geophysical Research 108, 3281, doi:10.1029/2002JC001.

Song, Y.T., Haidvogel, D.B., Glenn, S.M., 2001. Effects of topographic variability on the formation of upwelling centers off New Jersey: a theoretical model. Journal of Geophysical Research 106, 9223–9240.

Stewart, R.H., Joy, J.W., 1974. HF radio measurements of surface currents. Deep-Sea Research 21, 1039–1049.

Tilburg, C.E., Garvine, R.W., 2003. Three-dimensional flow in a shallow coastal upwelling zone: alongshore convergence and divergence on the New Jersey shelf. Journal of Physical Oceanography 33, 2113–2125.

Ullman, D.S., O'Donnell, J., Kohut, J., Fake, T., Allen, A., 2006. Trajectory prediction using HF radar surface currents: Monte Carlo simulations of prediction uncertainties. Journal of Geophysical Research 111, C12005, doi:10.1029/2006JC003715.

Winant, C.D., Beardsley, R.C., Davis, R.E., 1987. Moored wind, temperature, and current observations made during Coastal Ocean dynamics experiments 1 and 2 over the northern California shelf and upper slope. Journal of Geophysical Research 92, 1569–1604.

Yankowsky, A.E., Garvine, R.W., 1998. Subinertial dynamics on the inner New Jersey shelf during the upwelling season. Journal of Physical Oceanography 28, 2444–2458.

Yankovsky, A.E., Garvine, R.W., Münchow, A., 2000. Mesoscale currents on the inner New Jersey shelf driven by the interaction of buoyancy and wind forcing. Journal of Physical Oceanography 30, 2214–2230.